A COMPUTER AIDED DETECTION SYSTEM FOR CEREBRAL MICROBLEEDS IN BRAIN MRI

Babak Ghafaryasl[1], *Fedde van der Lijn*[1], *Mariëlle Poels*[2,3], *Henri Vrooman*[1], *Mohammad Arfan Ikram* [2,3], *Wiro J. Niessen*[1,5], *Aad van der Lugt*[2], *Meike Vernooij*[2,3] *and Marleen de Bruijne*[1,4]

[1]Biomedical Imaging Group Rotterdam, Department of Radiology & Medical Informatics, Erasmus MC, Rotterdam, the Netherlands

[2] Department of Radiology Erasmus MC, Rotterdam, the Netherlands

[3] Department of Epidemiology, Erasmus MC, Rotterdam, the Netherlands

[4]Department of Computer Science, University of Copenhagen, Denmark

[5]Imaging Science & Technology, Faculty of Applied Sciences, Delft University of Technology, Delft, the Netherlands

ABSTRACT

Advances in MR technology have improved the potential for visualization of small lesions in brain images. This has resulted in the opportunity to detect cerebral microbleeds (CMBs), small hemorrhages in the brain that are known to be associated with risk of ischemic stroke and intracerebral bleeding. In this paper, we propose a computer aided detection (CAD) system for the detection of CMBs to speed up visual analysis. Our method consists of three steps: (i) skull-stripping (ii) initial candidate selection and (iii) reduction of false-positives (FPs) using a two layer classification. Geometrical, intensity-based and local image descriptor features were used in the classification steps. The training and test set consist of 156 subjects (448 CMBs) and 81 subjects (183 CMBs), respectively. The sensitivity for CMB detection was 91% with, on average, 4.1 false-positives per subject.

Key words: brain MRI, cerebral microbleeds, classification, computer aided diagnosis.

1. INTRODUCTION

Cerebral microbleeds (CMBs) are hemosiderin deposits in the brain that are presumed to be caused by leakage of red blood cells from small blood vessels [1]. These microbleeds can be visualized on MRI sequences that are susceptible to hemosiderin depositions, i.e. T2*-weighted sequences. CMBs are known to be highly prevalent in patients admitted with ischemic stroke or intracerebral bleeding and are possibly related to worse outcome of these diseases [2]. Furthermore, it was recently shown that microbleeds are also common in the general elderly population, and that their location in the brain may indicate the underlying etiology [3].

Visual rating of CMBs is a tedious task, as it requires the observer to scroll through hundreds of thin slices in order to detect these hypointense small foci and to distinguish these from vessels. Also, there are other structures such as calcium and iron deposits which may mimic CMB and make the task more difficult [1]. Therefore, automated methods for CMB detection are of large interest, especially within the context of large imaging studies. CMBs can be recognized on MRI according to the following characteristics [1]: (1) hypointense spherical lesions on T2*-Weighted MRI (2) absence of signal hypointensity on proton density (PD)-weighted sequence (3) location in the brain parenchyma (grey or white matter) and not in cerebral spinal fluid (CSF).

We present a framework for detection of CMBs in T2*- and PD-weighted MR images, which is trained and evaluated on imaging data acquired within a large population-based study. The system decreases the workload for the observer by selecting a small number of CMB candidates. The proposed method identifies CMB candidates by thresholding the image and filtering the resulting connected components by size. These candidates are then labeled as CMB and non-CMB using a two-stage classification scheme.

2. METHOD

After preprocessing the method uses three stages to find the CMBs in a scan. First regions of interest containing CMB candidates are found, followed by two supervised classification steps. In the first classification step, the identified candidates were labeled using simple intensity, size, and shape features. This step will remove most of the false detections, while computation time for these features is low. The remaining candidates were used as the input for a second classification step which uses local image descriptors as features. These features are more expensive in computation time. The intensity features of PD-weighted sequences were also used in the second classification step to improve the result.

Preprocessing As a preprocessing step, the T2*- and PD-weighted images were first corrected for MR bias field artifacts using N3 [4]. The PD-weighted image was then rigidly

registered to the T2*-weighted image using the Elastix [5] software[2]. Finally skull-stripping of the T2*-weighted image was performed using the Brain Extraction Tool (BET) from the FSL package [6].

Candidate selection Microbleeds are visible on T2*-weighted images as low intensity foci with a specific size range. A binary image was produced by thresholding the intensity values of the T2*-weighted image. To find the region of interests(ROI), the bounding-box of connected components were filtered by size to remove unrealistically large or small candidates. All three thresholds were optimized using the training set.

First classification step The resulting ROIs in the previous stage were then labelled as CMB and non-CMB based on 17 simple geometric- and intensity-based features. The following seven size and shape features were extracted from the binarized and segmented images similar to [7]:

- The volume of the candidates: *vol*,
- The minimum, maximum and median length (in mm) of the boundingbox containing the candidate: $l_{min}, l_{max}, l_{med}$,
- The ratio of l_{min}/l_{max} and l_{max}/l_{med},
- Compactness: $vol/(l_{min} * l_{med} * l_{max})$.

The compactness and length ratios represent a measure of sphericity of the candidates, whereas the other features quantify size.

The intensity features used in this stage were the average, minimum, maximum, median, and standard deviation of the intensity values within the candidate ROIs. Additionally, the five intensity features were also calculated on dilated CMB candidates ROIs. We used a spherical morphology element with a diameter of 3 voxels for this aim.

To reduce the dimensionality of the resulting feature space, feed-forward feature selection (FFFS) was performed with the area under the receiver operating characteristic (ROC) curve as criterion. For the first step we considered a linear discriminant classifier (LDC), a quadratic discriminant classifier (QDC), and a Parzen classifier. All classifiers were implemented in the PRTOOLS pattern recognition toolbox for MATLAB.[1]

Second classification step The second classification stage is based on 38 features. The first 33 features are descriptors of local image structure. Since the CMBs appear in different sizes, it is essential to compute local image structure features at different scales. We applied several second order image structure features computed at different scales that can discriminate between spherical (CMBs structures), tubular, and plate-like local structure [7, 8, 9]. The list of the scale-space features that were extracted is shown in Table 1. Based on the size of the microbleeds we computed three different scales with in-plane dimensions of 0.5, 1, and 2 voxels. The value of vesselness parameters α, β and C were set as 0.5, 0.5 and 1220, respectively [8].

Since blood vessels caused a large amount of false positives in the previous classification step, we also added PD-based features to the second classifier to improve the results. The CMBs in the PD sequences are not clearly visible in the PD images but the blood vessels can be detected as the low intensity values in the image. For this purpose we computed the average, minimum, maximum, median, and standard deviation of the PD-weighted intensity values within the candidate ROI.

Table 1. Multiscale image features :

Description	
Computed at multiple scales:	
Eigen values of Hessian ($\lvert\lambda_1\rvert \geq \lvert\lambda_2\rvert \geq \lvert\lambda_3\rvert$)	λ_1,λ_2,λ_3
Ratios of Eigen values	$\frac{\lambda_1}{\lambda_2}$, $\frac{\lambda_1}{\lambda_3}$, $\frac{\lambda_2}{\lambda_3}$
Vesselness [8]	
Trace of Hessian	
Determinant of Hessian	
Trace of Hessian$\times$Hessian	
Determinant of Hessian$\times$Hessian	

In the second classification step, feature selection was performed in a similar way as in the first classification step by FFFS. For the second step four different classifiers were tested: a LDC, QDC, Parzen classifier, and a support vector classifier (SVC) with a linear kernel.

3. EXPERIMENT AND RESULTS

In this work image data was used from 237 elderly subjects (mean age 79.2) taken from a large population-based study [10]. This set contained, in total 631 microbleeds, 1 to 10 CMBs per scan. The images were acquired with a 1.5T (GE Healthcare) scanner using an eight-channel head coil. We used the 3D T2*-weighted and gradient recalled echo (GRE) PD-Weighted for our experiments. The slice thickness of the scans was 1.6 mm for T2*-weighted and PD-Weighted sequences which after zero-padding was interpolated to 0.8 mm. Voxel resolution was $0.5 \times 0.5 \times 0.8mm^3$. All of the CMBs in the 237 scans were manually labeled by two experienced reviewers independently and their labeling results were reviewed and scored for confirmation by an experienced neuroradiologist. The interobserver reliability was tested for microbleed rating by using Cohen κ test. Interobserver reli-

[2]http://elastix.isi.uu.nl/

[1]http://prtools.org/

abilities for the studies that were evaluated by both reviewers were "very good" both when analyzed at rater level, with $\kappa = 0.85$, and at microbleed level with $\kappa = 0.82$.

We divided this database in a training and test set, containing 156 scans with 448 CMBs and 81 scans with 183 CMBs, respectively. To select features, to choose the optimal classifiers and to determine the thresholds of the classifiers' posterior probabilities, the experiments were first performed on the training set which are different from test set even in the subject level. For this purpose the training set was thresholded to extract 448 candidate ROIs that contained a CMB, and 1600 candidate ROIs ,from initial candidates, that contained no CMBs. Half of this set were used to train the classifier, whereas the other half was used to compute the performance of a particular system configuration. In the first classfication step the threshold of the posterior probability was based on the best performance while removing the desired number of false candidates. The best performance was achieved by Parzen classifier by removing 97% of the FPs while having 94% sensitivity. This sensitivity was set as the threshold for the first classification step. For the second classification step, the best performance was achieved by QDC in the training set.

After the optimal configuration was determined in this way, the classifiers were retrained on the entire training set and the method was applied on the test set. The accuracy of the system was estimated using the sensitivity and number of false positives obtained on this latter set. The classification results of the first classifier on the test set are shown in figure 1 (top). This free-response receiver operating characteristic (FROC) curve shows the sensitivity as a function of the average number of false-positives per subject.

Figures 1 (middle) shows the FROC curve for the second classification step. The cumulative result of all stages is shown in figure 1 (bottom).

The summary of the results on the test set at each detection stage and the cumulative results after each stage are shown in Table 2. In the candidate selection stage the sensitivity CMB detection on the test set was 98.4% with, on average, 705 false-positives per subject. Applying the first classifier resulted in 19 false-positives on average per image at a sensitivity of 93.9%. After the second classifier the sensitivity was 91% and on average 4.1 false positives were found per subject. Figure 2(a-c) shows some examples of successfully detected CMBs as well as some false positives. In Figure 2(d) as an example the slice from the PD-weighted scan corresponding to image 2(c) is shown.

4. CONCLUSION AND DISCUSSION

We have presented a CAD system for automatic detection of cerebral microbleeds in MR images using a multistage classifier. The system was tested on a large database of 237 subjects taken from a population-based study. The method resulted in

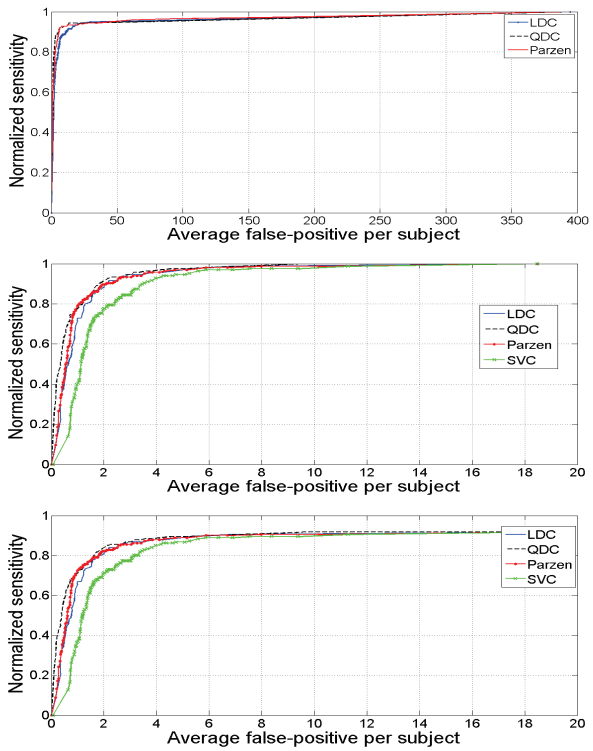


Fig. 1. FROC curves for test set: (top) the first classification step (middle) the second classification step and (bottom) the cumulative result of all three stages.

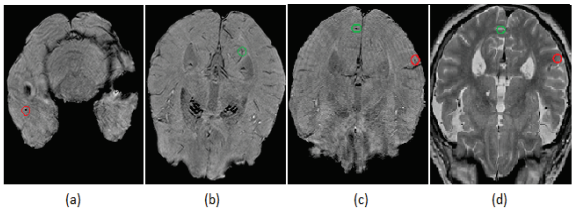


Fig. 2. some examples of successfully detected CMBs as well as some false positives (the red and green circles show the true-positives and false-positives respectively) (a)-(c) detected true-positives and false-positives on axial view of T2*-weighted MRI (d) The slice from the PD-weighted scan corresponding to image c

	Initial Candidate Selection	After First Classification Step Using Parzen	After Second Classification Step Using QDC
%Sensitivity	98.4	94	98.6
Average FP	705	19	4.1
%Cumulative Sensitivity	98.4	92.4	90.9

Table 2. Classification results on the test set

an average of 4.1 false positives per scan while maintaining a sensitivity of 91%.

Seghier et al. [11] proposed a technique for CMBs detection by using the mixture of Gaussians. However the accuracy of this technique is still low specially in the subjects with single CMBs. Kuijf et al. [12] proposed a technique using the radial symmetry transform for CMBs detection in 7T MRI images. However their technique is only evaluated by two subjects including 4 CMBs in total. Barnes et al. [13] proposed a technique based on different intensity and geometrical features which are used for training a support vector classifier for detecting CMBs in 1.5T MRI. The sensitivity of their technique is 81.7% with, on average, 107.5 false-positives per subject. Compare to these works our method shows a better performance and was validated on a larger database.

The main sources of false positives were blood vessels. Some examples of FPs are shown in figure 2. The other image descriptor features in PD sequences may cause to improve the results which will be included in future work. With the current amount of false positives, the proposed method cannot be used as a fully automated system. However, the system does reduce the amount of candidates to a level that can be visually inspected. The current system could therefore be useful to speed up manual annotation of CMBs by presenting the user only with the detected candidates.

5. ACKNOWLEDGEMENTS

This work is partly funded by the Netherlands Organisation for Scientific Research (NWO).

6. REFERENCES

[1] S.M. Greenberg, M.W. Vernooij, C. Cordonnier, A. Viswanathan, R. Al-Shahi Salman, S. Warach, L.J. Launer, M.A. Van Buchem, and M.M. Breteler. Cerebral microbleeds: a guide to detection and interpretation. *Lancet Neurol*, 8(2):165–74, 2009.

[2] W. Kakuda, VN Thijs, MG Lansberg, R. Bammer, L. Wechsler, S. Kemp, ME Moseley, MP Marks, and GW Albers. Clinical importance of microbleeds in patients receiving IV thrombolysis. *Neurology*, 65(8):1175, 2005.

[3] M.M.F. Poels, M.W. Vernooij, M.A. Ikram, A. Hofman, G.P. Krestin, A. Van Der Lugt, and M. Breteler. Prevalence and risk factors of cerebral microbleeds. *Stroke*, 41(10 suppl 1):S103–S106, 2010.

[4] J.G. Sled, A.P. Zijdenbos, and A.C. Evans. A nonparametric method for automatic correction of intensity nonuniformity in MRI data. *IEEE Transactions on Medical Imaging*, 17(1):87–97, 2002.

[5] S. Klein, M. Staring, K. Murphy, M.A. Viergever, and J.P.W. Pluim. Elastix: a toolbox for intensity-based medical image registration. *IEEE Transactions on Medical Imaging*, 29(1):196–205, 2010.

[6] S.M. Smith, M. Jenkinson, M.W. Woolrich, C.F. Beckmann, T.E.J. Behrens, H. Johansen-Berg, P.R. Bannister, M. De Luca, I. Drobnjak, D.E. Flitney, et al. Advances in functional and structural MR image analysis and implementation as FSL. *Neuroimage*, 23:208–219, 2004.

[7] K. Murphy, B. Van Ginneken, AMR Schilham, BJ De Hoop, HA Gietema, and M. Prokop. A large-scale evaluation of automatic pulmonary nodule detection in chest CT using local image features and k-nearest-neighbour classification. *Medical Image Analysis*, 13(5):757–770, 2009.

[8] A.F. Frangi, W.J. Niessen, K.L. Vincken, and M.A. Viergever. Multiscale vessel enhancement filtering. *Lecture Notes in Computer Science*, pages 130–137, 1998.

[9] P. Lo, J. Sporring, H. Ashraf, J.J.H. Pedersen, and M. de Bruijne. Vessel-guided airway tree segmentation: A voxel classification approach. *Medical Image Analysis*, 14(4):527–538, 2010.

[10] MW Vernooij, A. Van Der Lugt, MA Ikram, PA Wielopolski, WJ Niessen, A. Hofman, GP Krestin, and MMB Breteler. Prevalence and risk factors of cerebral microbleeds. *Neurology*, 70(14):1208–1214, 2008.

[11] M.L. Seghier, M.A. Kolanko, A.P. Leff, H.R. Jäger, S.M. Gregoire, and D.J. Werring. Microbleed detection using automated segmentation (MIDAS): A new method applicable to standard clinical MR images. *PloS one*, 6(3):e17547, 2011.

[12] H.J. Kuijf, J. de Bresser, G.J. Biessels, M.A. Viergever, and K.L. Vincken. Detecting cerebral microbleeds in 7.0 T MR images using the radial symmetry transform. In *Biomedical Imaging: From Nano to Macro, 2011 IEEE International Symposium on*, pages 758–761. IEEE, 2011.

[13] S.R.S. Barnes, E.M. Haacke, M. Ayaz, A.S. Boikov, W. Kirsch, and D. Kido. Semiautomated detection of cerebral microbleeds in magnetic resonance images. *Magnetic Resonance Imaging*, 29(6):844–52, 2011.